Postfault Operation Strategy With Minimum Harmonic Injection for Cascaded H-Bridge Inverters Driving a Multiphase Motor

Óscar López, *Senior Member, IEEE*, Jacobo Álvarez, Alejandro G. Yepes, *Senior Member, IEEE*, Martín Medina-Sánchez, and Jesús Doval-Gandoy, *Member, IEEE*

***Abstract*—Multiphase motor drives based on cascaded H-bridge (CHB) voltage source inverters (VSIs) offer enhanced reliability by accommodating both motor and VSI faults. The VSI faults, the most prevalent type, can be addressed by bypassing damaged H-Bridges. However, operating the VSI in this condition without an appropriate postfault strategy can increase the torque ripple and losses, and reduce the maximum motor speed. While conventional postfault strategies for three-phase CHB VSIs can be extended to more phases, they often result in a suboptimal performance because the extra degrees of freedom available in multiphase motors are ignored. Recently, these degrees of freedom have been exploited for the postfault operation of n-phase CHB VSIs to maximize the drive speed range without field weakening or torque ripple. However, excessive low-order xy harmonics arose in the stator current, producing a significant increase in its copper losses, which were limited by the use of a bulky filter. This article proposes a novel postfault operation strategy for n-phase CHB VSIs that dramatically reduces the stator copper losses by minimizing the injection of low-order xy harmonics in the stator voltage, effectively eliminating the filter requirement, while maintaining a wide speed range without field weakening or torque ripple. Experimental results obtained with a five-level five-phase motor drive corroborate the theoretical findings. This article is accompanied by a MATLAB script with the proposed strategy coded for the five-phase case.**

***Index Terms*—Carrier-based pulse-width modulation, multiphase drive, stator copper losses, voltage source inverters (VSI).**

I. Introduction

PRODUCTION losses in industrial high-power medium-voltage motor drives can be alleviated by adopting fault-tolerant drives with an adequate postfault operation strategy [1], [2]. A drive offering exceptional fault tolerance is the multiphase motor drive based on a Cascaded H-bridge (CHB) voltage source inverter (VSI), depicted in Fig. 1 [3]. The CHB VSI is a multilevel topology in which each phase consists of a string of equal power cells connected in series [4]. This modular structure enables the bypassing of damaged cells without stopping the motor [5], [6], bringing nearly continuous operation when an adequate hardware or software postfault strategy is adopted [1], [3], [7], [8], [9], [10], [11], [12], [13].

Hardware postfault strategies rely on adding redundant power cells to each phase [7], [8]. These cells remain inactive during normal operation. After a fault occurs, the damaged cell is bypassed, and its function is taken over by a redundant one [8]. As the number of phases increases, the cost and volume of the VSI also grow due to the presence of these idle cells. Conversely, software strategies do not require additional hardware, which is

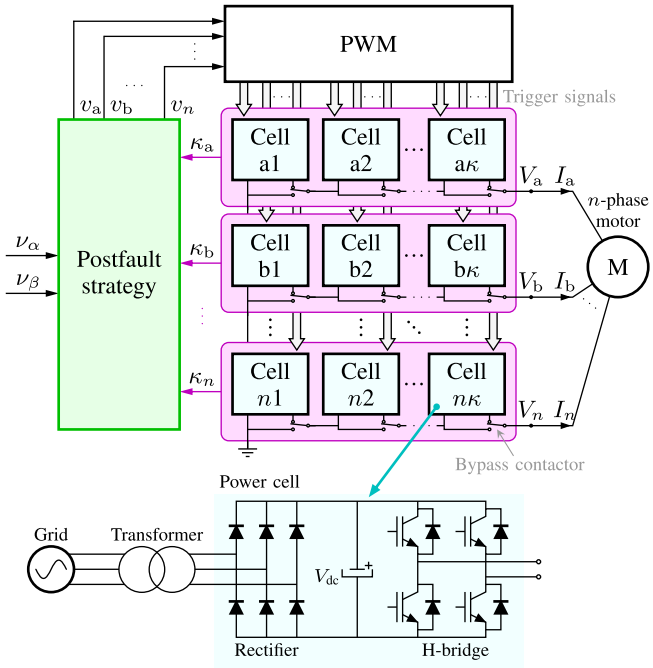

Fig. 1. Fault-tolerant n-phase motor drive based on a CHB VSI with κ cells per phase, where ν_α and ν_β are the $\alpha\beta$ components of the desired stator voltage, and κ_i and v_i stand for the number of nonbypassed cells and the pulse-width modulation (PWM) reference, respectively, corresponding to phase i.

Received 10 January 2024; revised 22 May 2024 and 24 July 2024; accepted 31 August 2024. Date of publication 9 September 2024; date of current version 12 December 2024. This work was supported in part by the FEDER under Grant MCIN/AEI/10.13039/501100011033 and in part by the UE under Grant PID2021-124136OB-I00. Funding for open access charge: Universidade de Vigo/CRUE-CISUG. Recommended for publication by Associate Editor Dian Guo (Co-EIC) Xu. *(Corresponding author: Óscar López.)*

The authors are with the Applied Power Electronics Technology Research Group, CINTECX, Universidade de Vigo, 36310 Vigo, Spain (e-mail: olopez@uvigo.gal; jalvarez@uvigo.gal; agyepes@uvigo.gal; martindamian.medina@uvigo.gal; jdoval@uvigo.gal).

This article has supplementary material provided by the authors and color versions of one or more figures available at https://doi.org/10.1109/TPEL.2024.3456390.

Digital Object Identifier 10.1109/TPEL.2024.3456390

especially beneficial in multiphase drives; however, they have to manage the VSI imbalance and the output voltage limitations that arise in the phases with bypassed cells [1]. A simple software approach is to bypass an equal number of cells in all phases [1], [9]. However, this wastes some useful healthy cells. The most effective software strategies are those that take advantage of all the healthy cells in the CHB VSI during the fault [1], [3], [10], [11]. Three-phase strategies typically inject a zero sequence into the pulsewidth modulation (PWN) references [1], [10], [11]. This injection can be performed by phase-shifting the fundamental of the PWM references, as shown in [1] with a successful industrial application [7]. This strategy is improved in [10] by adapting the PWM reference amplitudes, in addition to the phase shift. However, the optimal zero-sequence injection is achieved with the strategy by Carnielutti et al. [11], which maximizes the instantaneous stator voltage without introducing distortion in the flux/torque-producing ($\alpha\beta$) components. This translates to potentially maximize the motor speed without requiring field weakening or introducing torque ripple. This optimal strategy is extended for more than three phases in [3], which concluded that ignoring the extra degrees of freedom available in multiphase motors [14] leads to an unnecessary reduction in achievable speed. Such degrees of freedom are exploited by the minimum infinity-norm (MIN) postfault strategy, introduced in [3], to theoretically maximize the multiphase motor speed without flux weakening. This is accomplished by injecting the appropriate zero sequence and nonflux/torque producing (xy) components into the PWM reference to minimize its peak value without distorting the $\alpha\beta$ components, provided the stator windings are distributed. These injected xy voltages introduce low-order harmonics into the stator currents, which produce small (leakage) flux that minimally couples with the rotor [15], [16]. Consequently, they primarily affect the stator copper losses, with their impact on rotor and core losses being very limited [16] and often neglected [3], [17], [18], [19], [20], [21], [22]. However, if these currents are sufficiently high they can lead to unacceptable additional stator copper losses, necessitating the installation of a hardware xy filter [3]. Thus, to minimize extra stator losses and, consequently, filter size, it is essential to reduce the xy components injected into the PWM reference signals.

The minimization of the xy components for healthy two-level five-phase VSIs is investigated in [17], [18], [21], [23], where optimization problems are solved to constrain the PWM references and effectively prevent the modulator saturation, thereby avoiding distortion in the $\alpha\beta$ components. These investigations are subsequently extended for n-phase symmetrical motors in [22], showing that the minimization of the xy components of the PWM reference signals leads to a drastic reduction of the stator copper losses. All the aforementioned techniques exploit the existing symmetry in healthy two-level multiphase drives in order to solve the minimization problem in a reduced number of scenarios (e.g., a few regions in the first sector of the $\alpha\beta$ plane [18]). However, such symmetry is lost when the CHB VSI becomes unbalanced due to the bypassed cells [3], rendering the offline optimization approach impractical due to the overwhelming number of scenarios that must be considered, encompassing all possible configurations of bypassed cells. Consequently, none of the existing two-level multiphase strategies can be extended to the case of CHB VSI with bypassed cells. Therefore, the only postfault strategy identified in the literature that exploits the degrees of freedom of multiphase motors and is suitable for this specific kind of VSI is the aforementioned MIN strategy.

This article proposes a novel postfault operation strategy for multiphase CHB VSIs with bypassed cells that calculates online the PWM references with minimum injection of xy harmonic components and no $\alpha\beta$ distortion. Compared with state-of-the-art method (i.e., MIN), this new approach significantly reduces stator copper losses and consequently eliminates the need for an xy filter, while maintaining the to theoretical maximum speed without flux weakening or torque ripple.

The rest of this article is organized as follows. Section II reviews the model of a multiphase motor drive with bypassed cells in the CHB VSI, states the optimization problem, presents the new postfault strategy and illustrates its application with a small example. The new technique, designated as minimum xy (MXY) strategy, is analyzed and compared with the MIN strategy [3] by simulation in Section III, and experimentally, without an xy filter, in Section IV. Finally, Section V concludes this article.

II. Postfault MXY Injection Strategy

A. Multiphase Motor Drive With Bypassed Cells

The mathematical model of a multiphase motor is simplified if, under certain assumptions, the electrical variables are expressed in an orthogonal coordinate system defined by the generalized Clarke transformation $\mathbf{C}$ [24]. This transformation decomposes the n-dimensional voltage, current, and flux vectors of a n-phase motor into $\alpha\beta$, xy and zero-sequence components [25]. Assuming the stator windings are sinusoidally distributed, the electromechanical energy conversion process depends only on the $\alpha\beta$ components of currents and flux, which can be controlled by means of the $\alpha\beta$ components of the stator voltages [24]. Therefore, disregarding the nonlinearities of the PWM and VSI, the reference voltage vector $\mathbf{v} \stackrel{\text{def}}{=} [v_1, v_2, \ldots, v_n]^{\mathrm{T}}$, which gathers the PWM reference for each phase v_i, must obey the following equality constraints:

$$\nu_\alpha = \mathbf{c}_\alpha \mathbf{v} \tag{1a}$$

$$\nu_\beta = \mathbf{c}_\beta \mathbf{v} \tag{1b}$$

where ν_α and ν_β are the desired $\alpha\beta$ components for the stator voltage (which are provided by the drive controller), and $\mathbf{c}_\alpha$ and $\mathbf{c}_\beta$ are the rows in $\mathbf{C}$ that permit to calculate such components for a given n-dimensional vector $\mathbf{v}$.

Other voltage components different from ν_α and ν_β can be added to $\mathbf{v}$ since they do not affect the torque, the air-gap flux [14] nor the core and rotor losses [16], [20]. In principle, the zero-sequence voltage components can be injected without restriction because they do not produce additional stator currents, provided the neutrals of the stator windings are isolated [2]. On the contrary, the xy voltage injection should be minimized due to the fact that they cause undesired stator current components that increase stator copper losses [14], [22]. Such minimization can

be stated in the form of a cost function defined as the weighted sum of all the injected xy components squared

$$q(\mathbf{v}) \stackrel{\text{def}}{=} \sum_{i\in\{\text{xy}\}} w_i(\mathbf{c}_i\mathbf{v})^2 \qquad \text{with all } w_i > 0 \tag{2}$$

where $\mathbf{c}_i$ is the ith row of $\mathbf{C}$, which permits to calculate one of the xy components of $\mathbf{v}$, and w_i is the corresponding weighting factor. Although the w_i values can be chosen arbitrarily, selecting them proportionally to the inverse of the impedance squared of the corresponding xy plane leads to a cost function that reflects the excess of the stator copper losses caused by the xy injection process [21]. This proportionality, particularly at high speeds where this injection typically occurs, can be expressed as $w_i \propto 1/(h_i L_{\text{ls}i})^2$, where h_i and $L_{\text{ls}i}$ are the dominant harmonic order and the stator leakage inductance corresponding to the ith xy component, respectively [21].

Obviously, $q(\mathbf{v})$ would be zero if no xy components were injected in $\mathbf{v}$. However, it is well known that injecting zero xy components may lead to a reference that the VSI cannot synthesize [3], [23], and therefore the VSI output voltage constraints need to be taken into consideration. In general, the phase i of a VSI can synthesize any PWM reference v_i between some lower and upper bounds

$$l_i \le v_i \le u_i \qquad \text{with } i \in \{1, 2, \ldots, n\}. \tag{3}$$

For the case of the CHB VSI in Fig. 1, these bounds are [3]

$$\begin{aligned} l_i &= -\kappa_i \\ u_i &= +\kappa_i \qquad \text{with } i \in \{1, 2, \ldots, n\} \end{aligned} \tag{4}$$

where κ_i is number of healthy (nonbypassed) cells in phase i.

B. Optimization Problem Statement

Equations (1)–(3) define an optimization problem that can be stated as

$$\begin{aligned} \underset{\mathbf{v}}{\text{minimize}} \quad & q(\mathbf{v}) = \frac{1}{2}\mathbf{v}^{\text{T}}\mathbf{Q}\mathbf{v} && \text{(5a)} \\ \text{subject to} \quad & \nu_\alpha = \mathbf{c}_\alpha\mathbf{v} && \text{(5b)} \\ & \nu_\beta = \mathbf{c}_\beta\mathbf{v} && \text{(5c)} \\ & l_i \le \mathbf{e}_i\mathbf{v} \le u_i \quad \text{for all} i \in \{1, 2, \ldots, n\} && \text{(5d)} \end{aligned}$$

where the factor $1/2$ is included for convenience, $\mathbf{Q}$ is the symmetric positive semidefinite matrix that results from rewriting the quadratic form defined in (2) in matrix format, and $\mathbf{e}_i \stackrel{\text{def}}{=} [0, \ldots, 1, \ldots, 0]$ is the standard unit vector whose components are all zero except for the ith one whose value is one. The solution of this problem is the optimal PWM reference vector $\mathbf{v}^* \stackrel{\text{def}}{=} [v_1^*, v_2^*, \ldots, v_n^*]^{\text{T}}$ that minimizes the xy injection.

Given that $\mathbf{Q}$ is positive (semi)definite and all the constraints are linear, the problem in (5) is an optimization problem called convex quadratic program [26]. Two effective methods to solve convex quadratic programs are the interior-point and the active-set methods. The latter are generally preferred when the number of unknowns and constraints is small (below hundreds) because they are easy to implement and provide an exact solution after a small number of iterations [26], [27].

The active-set methods are founded on the observation that equality-constrained problems are simpler to solve than inequality-constrained ones. These methods start by making a guess of the subset of inequality constraints in (5d) that are active (i.e., satisfied as equalities) at the solution $\mathbf{v}^*$. Next, a equality-constrained quadratic program is solved imposing such set of constraints and ignoring the rest

$$\begin{aligned} \underset{\mathbf{v}}{\text{minimize}} \quad & q(\mathbf{v}) = \frac{1}{2}\mathbf{v}^{\text{T}}\mathbf{Q}\mathbf{v} && \text{(6a)} \\ \text{subject to} \quad & \nu_\alpha = \mathbf{c}_\alpha\mathbf{v} && \text{(6b)} \\ & \nu_\beta = \mathbf{c}_\beta\mathbf{v} && \text{(6c)} \\ & l_i = \mathbf{e}_i\mathbf{v} \qquad \text{for all } i \in \mathcal{L} && \text{(6d)} \\ & u_i = \mathbf{e}_i\mathbf{v} \qquad \text{for all } i \in \mathcal{U} && \text{(6e)} \end{aligned}$$

where $\mathcal{L}$ and $\mathcal{U}$ are the sets containing the indexes of the inequality constraints that are active at the solution for the lower and upper boundaries, respectively. In other words, the set $\mathcal{L}$ ($\mathcal{U}$) includes the phases of the VSI that should be clamped to their minimum (maximum) output levels to achieve minimum xy harmonic injection. If the solution of (6) meets a subset of certain optimality conditions, it is accepted as the solution of the original problem in (5). Otherwise a different educated guess of $\mathcal{L}$ and $\mathcal{U}$ that avoids choices that will not lead to a solution is made, and the process is repeated.

The complete set of the aforementioned optimality conditions that any solution $\mathbf{v}^*$ of (5) must observe is

$$\begin{aligned} & \mathbf{Q}\mathbf{v}^* - \mathbf{c}_\alpha^{\text{T}}\lambda_\alpha - \mathbf{c}_\beta^{\text{T}}\lambda_\beta - \sum_{i\in\mathcal{L}} \mathbf{e}_i^{\text{T}}\mu_i + \sum_{i\in\mathcal{U}} \mathbf{e}_i^{\text{T}}\mu_i = \mathbf{0} && \text{(7a)} \\ & \mathbf{c}_\alpha\mathbf{v}^* = \nu_\alpha && \text{(7b)} \\ & \mathbf{c}_\beta\mathbf{v}^* = \nu_\beta && \text{(7c)} \\ & \mathbf{e}_i\mathbf{v}^* = l_i \qquad \text{for all } i \in \mathcal{L} && \text{(7d)} \\ & \mathbf{e}_i\mathbf{v}^* = u_i \qquad \text{for all } i \in \mathcal{U} && \text{(7e)} \\ & l_i \le \mathbf{e}_i\mathbf{v}^* \le u_i \qquad \text{for all } i \notin \mathcal{L}\cup\mathcal{U} && \text{(7f)} \\ & \mu_i \ge 0 \qquad \text{for all } i \in \mathcal{L}\cup\mathcal{U} && \text{(7g)} \end{aligned}$$

where λ_α, λ_β and μ_i are arbitrary constants called Lagrange multipliers [26]. The multipliers λ_α and λ_β correspond to the equality constraints (5b) and (5c), respectively, and each μ_i corresponds to the ith inequality constraint in (5d), which is active at the solution. It is important to note that (7a) to (7e) are the optimality conditions corresponding to the solutions of the equality-constrained problem in (6). Hence, the remaining conditions (7f) and (7g) are the aforementioned subset of optimality conditions that this solution has to meet to be also accepted as a solution of the original problem in (5).

C. Proposed Active-Set Method for MXY Injection

The proposed active-set method is based on the iterative method described in [26]. At each iteration k a guess of the active sets $\mathcal{L}_k$ and $\mathcal{U}_k$, called working sets, and a feasible guess

of the solution $\mathbf{v}_k$ are considered in order to compute the optimal step vector $\mathbf{p}_k^* \stackrel{\text{def}}{=} [p_{1,k}^*, p_{2,k}^*, \ldots, p_{n,k}^*]^{\mathrm{T}}$ that reaches the optimal solution from $\mathbf{v}_k$ such that

$$\mathbf{v}^* \stackrel{\text{def}}{=} \mathbf{v}_k + \mathbf{p}_k^*. \tag{8}$$

This optimal step is obtained by solving the following optimization subproblem that results from introducing the change of variable $\mathbf{v} = \mathbf{v}_k + \mathbf{p}_k$ into (6)

$$\underset{\mathbf{p}_k}{\text{minimize}} \quad \frac{1}{2}\mathbf{p}_k^{\mathrm{T}}\mathbf{Q}\mathbf{p}_k + (\mathbf{Q}\mathbf{v}_k)^{\mathrm{T}}\mathbf{p}_k \tag{9a}$$

$$\text{subject to} \quad \mathbf{c}_\alpha \mathbf{p}_k = \nu_\alpha - \mathbf{c}_\alpha \mathbf{v}_k \tag{9b}$$

$$\mathbf{c}_\beta \mathbf{p}_k = \nu_\beta - \mathbf{c}_\beta \mathbf{v}_k \tag{9c}$$

$$\mathbf{e}_i \mathbf{p}_k = 0 \qquad \text{for all} i \in \mathcal{L}_k \cup \mathcal{U}_k. \tag{9d}$$

Any solution of this equality-constrained subproblem must obey the following optimality conditions [26]:

$$\mathbf{Q}\mathbf{p}_k^* - \mathbf{c}_\alpha^{\mathrm{T}}\lambda_{\alpha,k} - \mathbf{c}_\beta^{\mathrm{T}}\lambda_{\beta,k} - \sum_{i\in\mathcal{L}_k} \mathbf{e}_i^{\mathrm{T}}\mu_{i,k} + \sum_{i\in\mathcal{U}_k} \mathbf{e}_i^{\mathrm{T}}\mu_{i,k} = -(\mathbf{Q}\mathbf{v})^{\mathrm{T}} \tag{10a}$$

$$\mathbf{c}_\alpha \mathbf{p}_k^* = \nu_\alpha - \mathbf{c}_\alpha \mathbf{v}_k \tag{10b}$$

$$\mathbf{c}_\beta \mathbf{p}_k^* = \nu_\beta - \mathbf{c}_\beta \mathbf{v}_k \tag{10c}$$

$$\mathbf{e}_i \mathbf{p}_k^* = 0 \qquad \text{for all } i \in \mathcal{L}_k \cup \mathcal{U}_k \tag{10d}$$

which form a system of linear equations that must be solved for $\mathbf{p}_k^*$, $\lambda_{\alpha,k}$, $\lambda_{\beta,k}$ and $\mu_{i,k}$, with $i \in \mathcal{L}_k \cup \mathcal{U}_k$. An effective solution method is proposed in the Appendix.

By adding the resulting $\mathbf{p}_k^*$ to $\mathbf{v}_k$, as per (8), the solution of the equality-constrained problem in (6) is obtained, which will also be a solution of the original problem if it meets the aforementioned subset of optimality conditions (7f) and (7g).

When (7f) is not satisfied, the obtained solution is unfeasible, which means that the VSI is unable to synthesize such PWM reference. In this case only a fraction of the optimal step $\mathbf{p}_k^* \stackrel{\text{def}}{=} [p_{1,k}^*, p_{2,k}^*, \ldots, p_{n,k}^*]^{\mathrm{T}}$ is advanced and a new feasible guess for the solution is calculated as

$$\mathbf{v}_{k+1} = \mathbf{v}_k + \delta_k \mathbf{p}_k^* \tag{11}$$

where δ_k is the step-length parameter, which is chosen to be the largest value in the range [0,1] leading to a $\mathbf{v}_{k+1}$ observing (7f). The value of δ_k can be computed considering that, according to (11), the ith component of the vector $\mathbf{v}_{k+1}$ is $v_{i,k+1} = v_{i,k} + \delta_k p_{i,k}^*$. Hence, if $p_{i,k}^*$ is positive, $v_{i,k+1} > v_{i,k}$; then, the upper bound u_i could potentially be surpassed, and the constraint $v_{i,k+1} \leq u_i$ must be observed, which leads to

$$\delta_k < \frac{u_i - v_{i,k}}{p_{i,k}^*} \qquad \text{if } p_{i,k}^* > 0. \tag{12}$$

Otherwise, if $p_{i,k}^*$ is negative, the lower bound l_i is the one that could potentially be surpassed, leading to

$$\delta_k < \frac{l_i - v_{i,k}}{p_{i,k}^*} \qquad \text{if } p_{i,k}^* < 0. \tag{13}$$

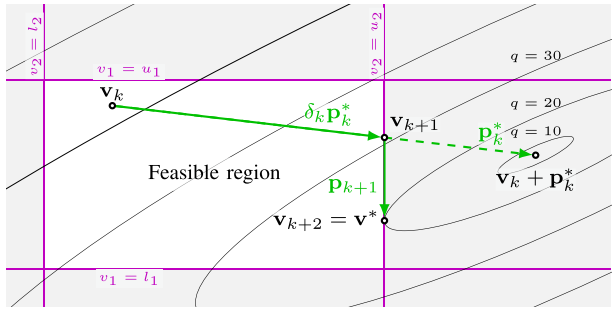

Fig. 2. Application of δ_k to prevent constraint violation. at iteration k: $\mathcal{L}_k = \mathcal{U}_k = \emptyset$. at iteration $k+1$: $\mathcal{L}_{k+1} = \emptyset$ and $\mathcal{U}_{k+1} = \{2\}$.

It is important to note that neither bound is surpassed if $p_{i,k}^*$ is zero because in this case the PWM reference for phase i $v_{i,k+1} = v_{i,k}$ is feasible, being this true for all clamped phases: $i \in \mathcal{L}_k \cup \mathcal{U}_k$. Consequently, the PWM reference vector $\mathbf{v}_{k+1}$ that results from (11) will observe (7f) by choosing the following step-length parameter:

$$\delta_k = \min_{i \notin \mathcal{L}_k \cup \mathcal{U}_k} \left(1, \min_{p_{i,k}^* > 0} \frac{u_i - v_{i,k}}{p_{i,k}^*}, \min_{p_{i,k}^* < 0} \frac{l_i - v_{i,k}}{p_{i,k}^*} \right). \tag{14}$$

The vector component i at which the above minimum occurs is called the blocking constraint and should be added to the corresponding working set before the next iteration as follows:

$$\mathcal{U}_{k+1} = \begin{cases} \mathcal{U}_k \cup \{i\} & \text{if } p_{i,k}^* > 0 \\ \mathcal{U}_k & \text{otherwise} \end{cases} \tag{15a}$$

$$\mathcal{L}_{k+1} = \begin{cases} \mathcal{L}_k \cup \{i\} & \text{if } p_{i,k}^* < 0 \\ \mathcal{L}_k & \text{otherwise.} \end{cases} \tag{15b}$$

Fig. 2 illustrates the application of δ_k to prevent constraint violation. At iteration k, advancing the optimal step $\mathbf{p}_k^*$ would lead to an unfeasible solution $\mathbf{v}_k + \mathbf{p}_k^*$, due to the violation of the constraint $v_2 \leq u_2$. To address this, only a fraction of this step is advanced up to the boundary $v_2 = u_2$, and this blocking constraint is included in the upper working set as $\mathcal{U}_{k+1} = \{2\}$. By activating this constraint, the optimal solution is finally reached in the subsequent iteration. When the last optimality condition (7g) is not satisfied, indicating the existence of some negative Lagrange multiplier $\mu_{i,k}$, the value of the cost function may be decreased by dropping some active constraints. In this case, the constraint j corresponding to the most negative Lagrange multiplier

$$j = \arg\min_i \mu_{i,k} \qquad \text{for } i \in \mathcal{L}_k \cup \mathcal{U}_k \tag{16}$$

is removed from the working sets as follows:

$$\mathcal{L}_{k+1} = \begin{cases} \mathcal{L}_k \backslash \{j\} & \text{if } j \in \mathcal{L}_k \\ \mathcal{L}_k & \text{otherwise} \end{cases} \tag{17a}$$

$$\mathcal{U}_{k+1} = \begin{cases} \mathcal{U}_k \backslash \{j\} & \text{if } j \in \mathcal{U}_k \\ \mathcal{U}_k & \text{otherwise.} \end{cases} \tag{17b}$$

TABLE I
PROPOSED ACTIVE-SET ALGORITHM FOR MXY INJECTION

Calculate l_i and u_i from κ_i according to (4);
Determine a feasible starting voltage vector $\mathbf{v}_0$;
Set $\mathcal{L}_0$ and $\mathcal{U}_0$ to be subsets of the active constraints at $\mathbf{v}_0$;
for $k = 0, 1, 2, \ldots$
  Solve (10) for the optimal step $\mathbf{p}_k^*$; *// See Table II.*
  if $\mathbf{p}_k^* \neq \mathbf{0}$ *// The optimal step is non−zero.*
    Compute δ_k from (14);
    Update $\mathbf{v}_{k+1} \leftarrow \mathbf{v}_k + \delta_k \mathbf{p}_k^*$; *// See (11).*
    if $\delta_k < 1$ *// There is a new blocking constraint.*
      Update $\mathcal{L}_{k+1}$ and $\mathcal{U}_{k+1}$ according to (15);
    else *// There is no new blocking constraint.*
      Keep $\mathcal{L}_{k+1} \leftarrow \mathcal{L}_k$ and $\mathcal{U}_{k+1} \leftarrow \mathcal{U}_k$;
    end if
  else *// The step is zero, thus condition (7f) is satisfied.*
    Solve (10) for the multipliers $\mu_{i,k}$; *// See Table II.*
    if $\mu_{i,k} \geq 0$ *// The last condition (7g) is satisfied.*
      stop with solution $\mathbf{v}^* = \mathbf{v}_k$ for the PWM reference;
    else *// Drop one constraint.*
      Update $\mathcal{L}_{k+1}$ and $\mathcal{U}_{k+1}$ according to (16) and (17);
      Keep $\mathbf{v}_{k+1} \leftarrow \mathbf{v}_k$;
    end if
  end if
end for

D. Proposed Active-Set Algorithm for MXY Injection

The algorithm developed to implement the proposed active-set method permits to calculate, at every switching cycle, the optimal PWM reference vector $\mathbf{v}^*$ for a given reference stator voltage $\boldsymbol{\nu} \stackrel{\text{def}}{=} [\nu_\alpha, \nu_\beta]^{\mathrm{T}}$, taking into account the number of nonbypassed cells in each phase κ_i (see Fig. 1). In what follows, the framed number $\boxed{j}$ indicates the matching line in the pseudocode listing outlined in Table I.

$\boxed{1}$ First, the boundaries l_i and u_i of the feasible voltage range for each phase i of the VSI are calculated from κ_i according to (4). $\boxed{2}$ Next, a feasible starting voltage vector $\mathbf{v}_0 = [v_{1,0}, v_{2,0}, \ldots, v_{n,0}]^{\mathrm{T}}$ is determined. Using a $\mathbf{v}_0$ close to the solution ("warm start") may expedite the algorithm convergence. A practical choice for the starting vector could be the solution obtained in the previous VSI switching cycle. However, any $\mathbf{v}_0$ that satisfies the inequality constraints in (5d) can be employed as starting vector when no information about the solution is available ("cold start"). $\boxed{3}$ Next, the initial working sets $\mathcal{L}_0$ are $\mathcal{U}_0$ are constructed by incorporating all (or part) of the indexes i for which $v_{i,0} = l_i$ or $v_{i,0} = u_i$, respectively. $\boxed{4}$ After that, an iterative process begins. $\boxed{5}$ At each iteration k, the system in (10) is solved for the optimal step $\mathbf{p}_k^*$, considering $\boldsymbol{\nu} = [\nu_\alpha, \nu_\beta]^{\mathrm{T}}$. This can be achieved by employing the method proposed in Appendix. $\boxed{6\text{-}8}$ If $\mathbf{p}_k^*$ is nonzero, the step-length parameter δ_k is calculated using (14) and the PWM reference vector is updated to $\mathbf{v}_{k+1}$ considering (11). $\boxed{9\text{-}10}$ If $\delta_k < 1$, the step along $\mathbf{p}_k^*$ is blocked by some constraint that is not currently in $\mathcal{L}_k$ or $\mathcal{U}_k$; thus, this new constraint is added to the appropriate working set according to (15). $\boxed{11\text{-}12}$ Otherwise, if $\delta_k = 1$, the step is not blocked, and the working sets are kept for the next iteration, meaning that $\mathcal{L}_{k+1} = \mathcal{L}_k$ and $\mathcal{U}_{k+1} = \mathcal{U}_k$.

TABLE II
PROPOSED METHOD TO CALCULATE THE OPTIMAL STEP VECTOR AND THE LAGRANGE MULTIPLIERS

Given $\mathbf{Q}$, $\mathbf{c}_\alpha$, $\mathbf{c}_\beta$, $\boldsymbol{\nu} = [\nu_\alpha, \nu_\beta]^{\mathrm{T}}$, $\mathbf{v}$, $\mathcal{L}$ and $\mathcal{U}$, obtain $\mathbf{A}$, $\mathbf{E}$ and calculate $\mathbf{h} = \mathbf{A}\mathbf{v} - \boldsymbol{\nu}$, according to (18);
Obtain $\bar{\mathbf{E}}$ according to (20);
Obtain $\hat{\mathbf{Q}} = \bar{\mathbf{E}}\mathbf{Q}\bar{\mathbf{E}}^{\mathrm{T}}$, $\hat{\mathbf{A}} = \mathbf{A}\bar{\mathbf{E}}^{\mathrm{T}}$ and $\hat{\mathbf{g}} = \bar{\mathbf{E}}\mathbf{Q}\mathbf{v}$, from (24);
Choose two independent columns of $\hat{\mathbf{A}}$ and obtain matrices $\mathbf{P}$, $\mathbf{M}$ and $\mathbf{N}$ according to (28);
Calculate $\mathbf{Y}$ and $\mathbf{Z}$ from (26) and (27), respectively;
Solve (30) for $\mathbf{z}$ with (31) or by Cholesky factorization;
Calculate $\hat{\mathbf{p}}^* = -\mathbf{Y}\mathbf{h} + \mathbf{Z}\mathbf{z}$, according to (25) and (29);
Calculate $\mathbf{p}^* = \bar{\mathbf{E}}^{\mathrm{T}}\hat{\mathbf{p}}^*$, according to (19);
Calculate $\boldsymbol{\lambda} = \mathbf{Y}^{\mathrm{T}}\hat{\mathbf{Q}}\hat{\mathbf{p}}^* + \mathbf{Y}^{\mathrm{T}}\hat{\mathbf{g}}$, according to (32);
Calculate $\boldsymbol{\mu} = \mathbf{E}\mathbf{Q}(\mathbf{v} + \mathbf{p}^*) - \mathbf{E}\mathbf{A}^{\mathrm{T}}\boldsymbol{\lambda}$, according to (23);

$\boxed{14}$ If $\mathbf{p}_k^* = \mathbf{0}$, then the vector $\mathbf{v}_k$ satisfies the optimality condition (7f). $\boxed{15}$ In this case, the Lagrange multipliers $\mu_{i,k}$ for all $i \in \mathcal{U}_k \cup \mathcal{L}_k$ are computed by solving (10), which can be done using the method in Table II. $\boxed{16\text{-}17}$ If the resulting $\mu_{i,k}$ are all nonnegative, the last optimality condition (7g) is satisfied, and therefore the algorithm terminates with the optimal solution $\mathbf{v}^* = \mathbf{v}_k$ for the PWM reference. $\boxed{18\text{-}19}$ Otherwise, a new iteration is carried out after dropping the constraint given by (16) from the working sets according to (17). $\boxed{20}$ For this new iteration, the PWM reference is maintained: $\mathbf{v}_{k+1} = \mathbf{v}_k$.

E. Example for a Faulty Five-Phase CHB VSI

The application of the proposed postfault strategy is illustrated for a five-phase ($n = 5$) CHB VSI with two power cells per phase when cell a1 is bypassed (see Fig. 1). In such situation, the numbers of nonbypassed cells per phase are $\kappa_a = 1$ and $\kappa_b = \kappa_c = \kappa_d = \kappa_e = 2$. Considering the amplitude-invariant Clarke transformation [24] and the weighting factors $w_x = w_y = 1$ for the cost function (2) leads to $\mathbf{c}_\alpha = [0.4, 0.124, -0.324, -0.324, 0.124]$, $\mathbf{c}_\beta = [0, 0.380, 0.235, -0.235, -0.380]$ and

$$\mathbf{Q} = \begin{bmatrix} 0.320 & -0.259 & 0.099 & 0.099 & -0.259 \\ -0.259 & 0.320 & -0.259 & 0.099 & 0.099 \\ 0.099 & -0.259 & 0.320 & -0.259 & 0.099 \\ 0.099 & 0.099 & -0.259 & 0.320 & -0.259 \\ -0.259 & 0.099 & 0.099 & -0.259 & 0.320 \end{bmatrix}.$$

Given a desired stator voltage vector[1] $\boldsymbol{\nu} = [\nu_\alpha, \nu_\beta]^{\mathrm{T}} = [1.308, 1.308]^{\mathrm{T}}$ p.u., the optimization problem stated in (5) becomes fully defined, and it is subsequently solved for $\mathbf{v}$ by following the steps outlined in Table I.

$\boxed{1}$ First, the calculation of the boundaries of the feasible voltage range for each VSI yields $l_a = -1$, $u_a = 1$, $l_b = l_c = l_d = l_e = -2$ and $u_b = u_c = u_d = u_e = 2$. $\boxed{2\text{-}3}$ Assuming a warm start with initial vector $\mathbf{v}_0 = [1, 0, 0, -2, -2]^{\mathrm{T}}$ p.u., the

[1]The normalization factor for voltages is the voltage step of the CHB VSI (i.e., 1 p.u. = V_{dc}), while for time variables, it is the fundamental period (i.e., 1 p.u. = 20 ms at 50 Hz).

initial subsets of the active constraints at $\mathbf{v}_0$, i.e., its clamped phases, are $\mathcal{L}_0 = \{d, e\}$ and $\mathcal{U}_0 = \{a\}$.

1) Iteration $k = 0$: 5 The application of the first eight instructions outlined in Table II yields the optimal step vector $\mathbf{p}_0^* = [0, 0.949, -1.208, 0, 0]^{\mathrm{T}}$ p.u. 6-7 Since $\mathbf{p}_0^* \neq \mathbf{0}$, the step-length parameter is calculated by using (14), which results in $\delta_0 = 1$. 8 Next, the PWM reference is updated to $\mathbf{v}_1 = [1, 0.949, -1.208, -2, -2]^{\mathrm{T}}$ p.u., according to (11). 11-12 Furthermore, since $\delta_0 = 1$, the working sets remain the same, which means $\mathcal{L}_1 = \{d, e\}$ and $\mathcal{U}_1 = \{a\}$.

2) Iteration $k = 1$: 5 From $\mathbf{v}_1$, the calculation of a new optimal step yields $\mathbf{p}_1^* = [0, 0, 0, 0, 0]^{\mathrm{T}}$ p.u. 14 Considering that $\mathbf{p}_1^* = \mathbf{0}$, the vector $\mathbf{v}_1$ is a potential solution of the optimization problem and the Lagrange multipliers associated with the phases in the set $\mathcal{L}_1 \cup \mathcal{U}_1$ must be determined. 15 This is done by following the last two steps described in Table II, which lead to $\mu_{a,1} = -0.0851$, $\mu_{d,1} = 0.747$ and $\mu_{e,1} = -0.562$. 18 The existence of negative multipliers reveals that $\mathbf{v}_1$ cannot be a solution of the problem. 19 As a result, the phase with the most negative multiplier (phase e) is dropped from the working sets, leading to $\mathcal{L}_2 = \{d\}$ and $\mathcal{U}_2 = \{a\}$. 20 Meanwhile, the PWM reference vector remains unchanged: $\mathbf{v}_2 = [1, 0.949, -1.208, -2, -2]^{\mathrm{T}}$ p.u.

3) Iteration $k = 2$: 5-8 & 11-12 The computation of the new optimal step vector from the PWM reference $\mathbf{v}_2$ results in $\mathbf{p}_2^* = [0, 0.568, 0.568, 0, 0.920]^{\mathrm{T}}$ p.u., which is nonzero. This leads to the step-length parameter $\delta_2 = 1$ and the new PWM reference $\mathbf{v}_3 = [1, 1.517, -0.639, -2, -1.080]^{\mathrm{T}}$ p.u., while the working sets do not change: $\mathcal{L}_3 = \{d\}$ and $\mathcal{U}_3 = \{a\}$.

4) Iteration $k = 3$: 5 The optimal step from $\mathbf{v}_3$ is found to be $\mathbf{p}_3^* = \mathbf{0}$, indicating that the Lagrange multipliers must be determined. 14-15 The multipliers for phases a and d result in $\mu_{a,3} = \mu_{d,3} = 0.1959$. 16 Since all multipliers are nonnegative, $\mathbf{v}_3$ is finally the solution of the problem. 17 Therefore, the algorithm terminates with the optimal PWM reference $\mathbf{v}^* = [1, 1.517, -0.639, -2, -1.080]^{\mathrm{T}}$ p.u., and with the phases d and a clamped to their minimum and maximum voltage levels, respectively.

III. Simulation Results

The proposed MXY postfault strategy is analyzed via simulation and compared with the MIN strategy [3] considering the amplitude-invariant Clarke transformation and the same parameters of the experimental setup, namely, five phases and two cells per phase. For convenience, it is assumed that the fault occurs in cell a1 (see Fig. 1), which represents a challenging scenario since the range of feasible output voltages for the corresponding phase is halved compared to the healthy condition. A single fault in any other phase would yield comparable results, due to symmetry. The supplementary material accompanying this article includes the MATLAB code for the postfault strategies compared in this section. Fig. 3 compares the results obtained with the MXY and the MIN postfault strategies for a sinusoidal stator voltage reference with an amplitude of 1.85 p.u. In a healthy condition, with no bypassed cells, MXY yields the same PWM reference as the generalized min–max injection technique by Carnielutti [3], [28], as expected. This is because in this situation, no xy injection is necessary, and the Carnielutti's method already provides an optimal solution. When cell a1 is bypassed ($\kappa_a = 1$), the boundaries of the feasible voltage range of phase a shrink from $l_a = -2$ p.u. and $u_a = 2$ p.u. to $l_a = -1$ p.u. and $u_a = 1$ p.u., respectively. In this fault scenario, the MXY strategy injects the minimum xy components necessary to prevent distorting the $\alpha\beta$ components, which results in the clamping of some VSI phases during some time intervals. In contrast, the behavior of the MIN strategy is completely different under the same scenario. The MIN strategy minimizes the peak values of the PWM references to avoid $\alpha\beta$ distortion, resulting in no phase clamping and, consequently, more xy component injection than it is strictly required. This conclusion is obtained by comparing the middle bottom plots in Fig. 3. The stator current components drawn by an induction motor that matches the experimental setup are plotted at the bottom of Fig. 3. The simulation results confirm that neither the MXY nor the MIN strategies introduces distortion in the $\alpha\beta$ current components. However, the MXY strategy injects significantly less xy current. Therefore, both techniques would produce the same torque profile, but the MXYstrategy offers the advantage of lower stator copper losses.

Fig. 4 plots the value of cost function $q(\mathbf{v})$, with weighting factors $w_x = w_y = 1$, averaged over a fundamental period, for the reference voltages obtained by using the MXY and MIN strategies up to $\|\boldsymbol{\nu}\| = \hat{v}_{\max}$, which is the maximum voltage achievable by the CHB VSI without $\alpha\beta$ distortion. The value of $\hat{v}_{\max}$ for any bypassed cell configuration was established in [3]. Assuming the motor can accommodate the injected xy currents, this voltage limit can be translated into the maximum speed achievable by the motor drive without field weakening, i.e., without torque derating, as $\hat{\omega}_{\max} = \hat{v}_{\max}\omega_r V_{\mathrm{dc}}/\sqrt{2}/V_r$ where ω_r is the rated motor speed and V_r is the rated motor voltage. In a healthy condition, the MXY strategy achieves zero cost, i.e., it does not perform xy injection, up to the theoretical maximum amplitude for the stator voltage reference $\|\boldsymbol{\nu}\| = \kappa/\cos(\pi/10) = 2.10$ p.u. [3], [23]. When one cell (a1) is bypassed, MXY begins injecting xy components at an amplitude of $\|\boldsymbol{\nu}\| \approx 1.58$ p.u. In contrast, the performance of the MIN strategy is significantly worse in this scenario, as it injects a substantially higher amount of xy components across the entire range of reference stator voltage amplitudes. When two cells in adjacent phases (a1 & b1) are bypassed, avoiding distortion in the $\alpha\beta$ components requires xy injection for amplitudes between 1.58 p.u. and 1.85 p.u. If $\|\boldsymbol{\nu}\|$ exceeds 1.85 p.u., such distortion would become unavoidable. The simulations also reveal that when the two bypassed cells are in nonadjacent phases (a1 and c1) the scenario is more challenging, as a substantially greater amount of xy component injection is required, which must be performed from $\|\boldsymbol{\nu}\| = 1.05$ p.u. up to $\|\boldsymbol{\nu}\| = 1.70$ p.u. This finding is consistent with the conclusions drawn from other articles studying the fault tolerance of five-phase motors [19]. Notably, in all fault scenarios, the MXY strategy achieves the theoretical maximum $\|\boldsymbol{\nu}\|$ attainable by the CHB VSI without distortion in the $\alpha\beta$ components $\hat{v}_{\max}$ [3]. However, other

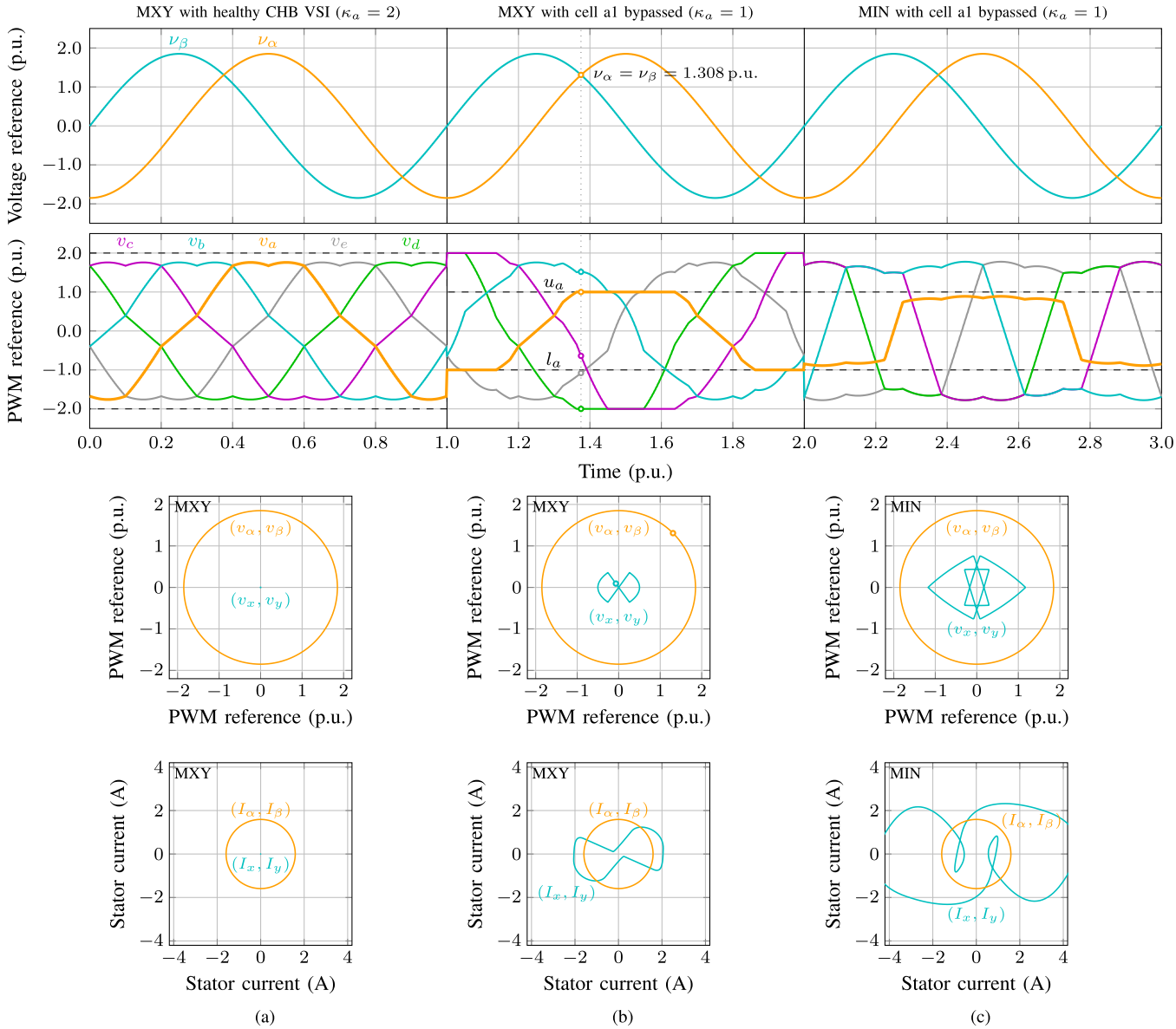

Fig. 3. PWM reference signals (middle) and stator currents (bottom) obtained for a reference stator voltage (top) with amplitude $\|\boldsymbol{\nu}\| = 1.85$ p.u. for (a) healthy situation with MXY, and fault scenario with cell a1 bypassed using (b) the MXY and (c) the MIN strategies. Dashed black lines show the lower l_a and the upper u_a boundaries of the range of feasible voltages for the phase a. The highlighted points correspond with the example in Section II-E.

practical limitations of the motor drive, such as machine overheating or limitations in the VSI output current, often are more restrictive. It is under these circumstances that the optimal xy injection performed by the MXY strategy largely widens the speed range compared with the MIN strategy, as will be shown in the experimental tests.

The MXY injection strategy, while advantageous, necessitates a demanding iterative computational process. The convergence of the for-loop within the algorithm in Table I, and consequently the computation time, depends on the starting voltage (cold/warm start) and the input vector $\boldsymbol{\nu}$. Fig. 5 shows the number of for-loop iterations needed to obtain the PWM reference for each switching cycle for the case in Fig. 3(b) (sinusoidal reference with $\|\boldsymbol{\nu}\| = 1.85$ p.u. and cell a1 bypassed) considering cold and warm starts. Cold starts use a zero initial vector $\mathbf{v}_0$ in all cycles, while warm starts utilize the optimal solution $\mathbf{v}^*$ from the prior cycle. The simulations show convergence within five iterations for both methods, but warm starts typically require only two iterations (2.067 average per cycle) compared to cold starts (3.315 average per cycle).

IV. Experimental Results

The proposed postfault strategy is evaluated with the same experimental setup used in [3], but without the bulky xy current filter. Fig. 6 depicts this setup, which consists of a five-phase induction motor drive mechanically coupled to a dc generator loaded with a resistor bank. The induction motor is rated for 110 V at 50 Hz, with a speed of 1380 r/min (8% slip). It features

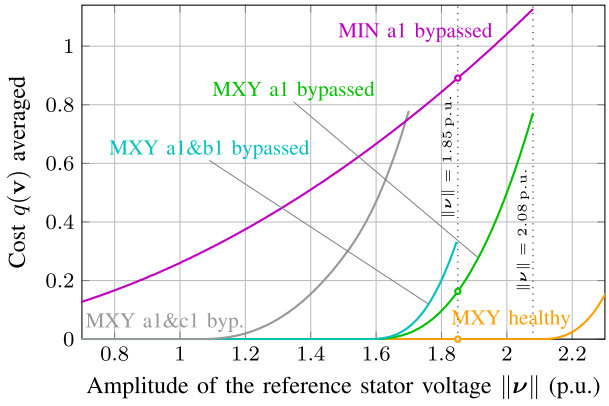

Fig. 4. Value of the cost function $q(\mathbf{v})$ averaged over a fundamental period with respect to the amplitude of the reference stator voltage $\|\nu\|$ without $\alpha\beta$ distortion. The highlighted points correspond to the simulations in Fig. 3.

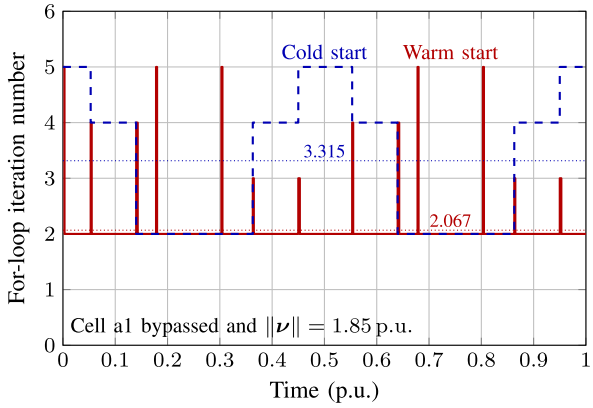

Fig. 5. For-loop iteration number within the algorithm of the MXY strategy with cold and warm start for 400 samples of a fundamental period when the cell a1 is bypassed and the amplitude of the reference stator voltage is $\|\nu\| = 1.85$ p.u.

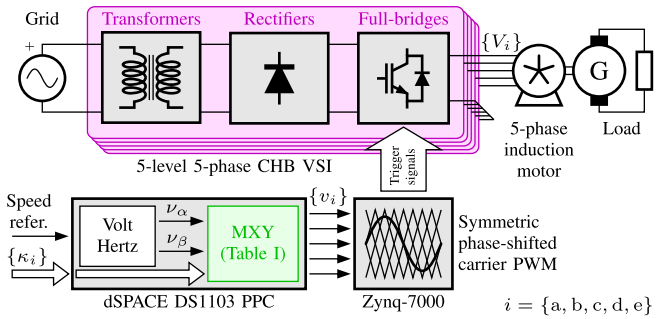

(a)

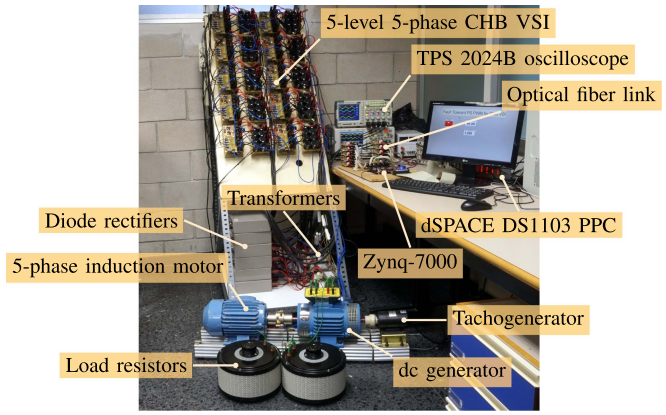

(b)

Fig. 6. Experimental test rig based on a five-level five-phase CHB VSI. (a) Block diagram. (b) Picture.

530-mH magnetizing inductance, 25-mH stator leakage inductance, 50-mH rotor leakage inductance, 9.5-Ω stator resistance, and 7.0-Ω rotor resistance. The CHB VSI employs two cells per phase ($\kappa = 2$). Each cell is an H-bridge constructed using four IRGB6B60KD insulated-gate bipolar transistors. The cells are supplied by a single-phase diode rectifier connected to a bank of aluminum electrolytic capacitors with a total capacitance of 940 μF. The dc-link voltage of each cell is $V_{\text{dc}} = 76$ V. The trigger signals transmitted by optical fiber to the transistor drivers are generated by a Xilinx Zynq-7000 system-on-chip using the symmetric regular sampled phase-shifted carrier PWM technique [29]. The transistors switch at 2.5 kHz with a 5-μs dead time. The PWM reference vectors $\mathbf{v}$ are computed using the postfault strategies under test by the PowerPC 604e of a dSPACE DS1103 PPC controller board. The reference stator-voltage vectors $\boldsymbol{\nu} = [\nu_\alpha, \nu_\beta]^{\text{T}}$ are calculated in open loop with the Volts/Hertz criterion [29]. No compensations for semiconductor voltage drops, dead times, or any other VSI nonlinearity [30] have been considered. Fig. 7 presents experimental results obtained with the MXY and MIN strategies for a stator voltage reference of amplitude $\|\nu\| = 1.4$ p.u. at 34 Hz and rated slip (8%).

The top captures show, for phases a and b of the VSI, the raw output voltages (V_a and V_b in Fig. 1), which exhibit five levels, and the same signals low-pass filtered ($\bar{V}_a$ and $\bar{V}_b$) with a cutoff frequency of 1.46 kHz. The filtered VSI output voltages for all phases are presented in the middle top oscilloscope captures. The stator currents (I_a, I_b, ... in Fig. 1) are shown in the middle bottom captures, whereas their $\alpha\beta$ and xy components are plotted at the bottom. The measurements in Fig. 7(a) correspond to the healthy VSI operation under the MXY strategy, which in this situation yields the same results as the generalized min–max injection by Carnielutti [3], [28]. The raw VSI output voltages have five levels, as usual [29], the stator currents form a balanced five-phase system, and their $\alpha\beta$ components trace a circular trajectory, while their xy components remain negligible. When the cell a1 is bypassed, the raw output voltage of phase a V_a becomes a three-level waveform. Fig. 7(b) shows that, using the MXY strategy in this scenario, the stator currents are roughly the same as in healthy condition. As a result, the $\alpha\beta$ components of the current still follow a circular trajectory and slight xy current components arise. Conversely, Fig. 7(c) proves that using the MIN strategy without an xy filter under the same fault scenario induces excessive xy stator currents, while the trajectory of the $\alpha\beta$ stator currents exhibits some distortion attributable to the inherent VSI nonlinearities. Notably, these measurements are consistent with the simulation outcomes presented in Fig. 4 for $\|\nu\| = 1.4$ p.u.

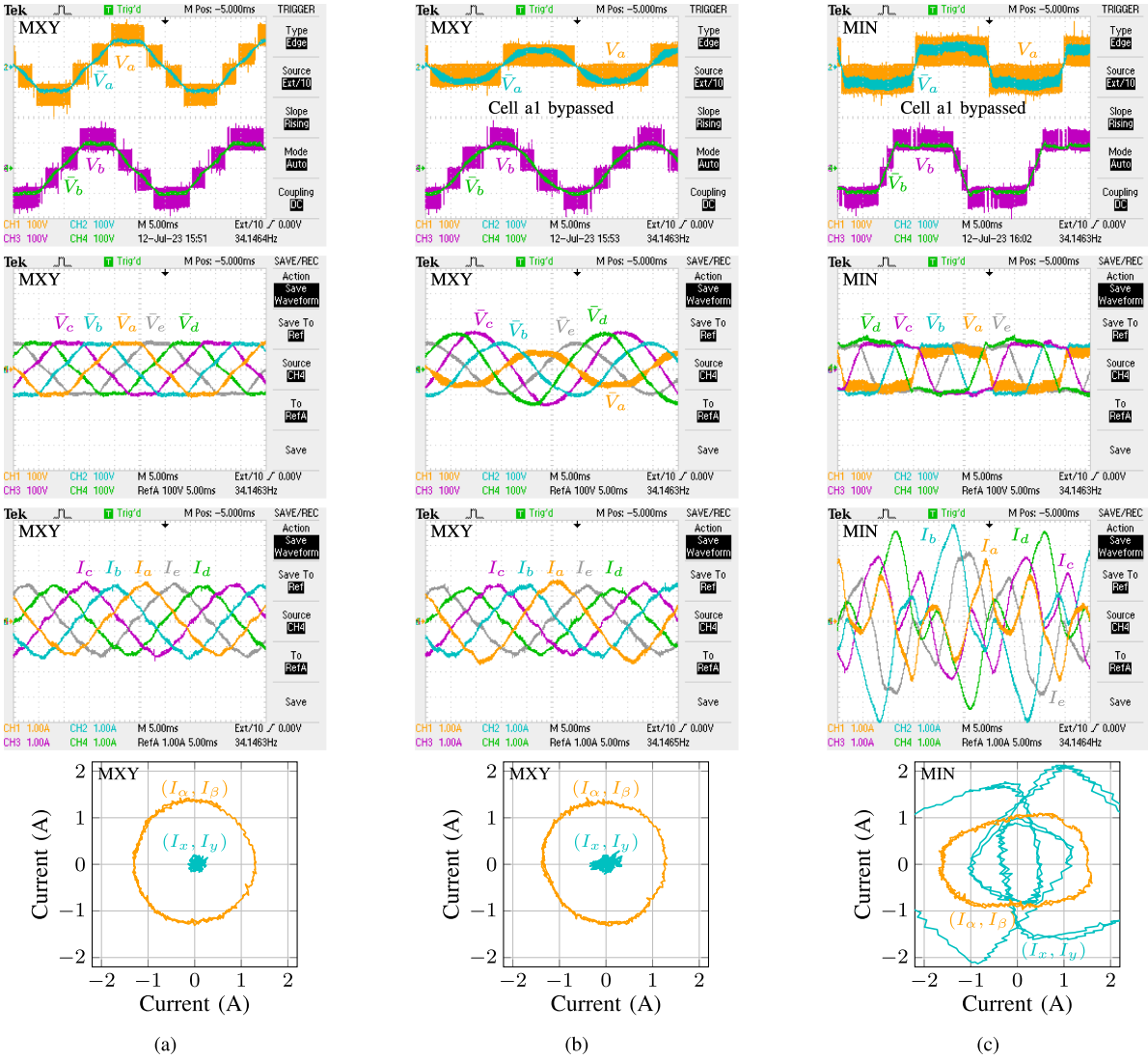

Fig. 7. Experimental measurements for $\|\boldsymbol{\nu}\| = 1.4$ p.u., 34 Hz and 8% slip. Raw VSI output voltages, with some waveforms omitted for clarity (top), filtered output voltages (middle top), raw stator currents (middle bottom) and $\alpha\beta$ and xy components of the stator currents (bottom). (a) Healthy VSI with MXY, and cell a1 bypassed with (b) MXY and (c) MIN.

The same test procedure is followed in Fig. 8 to examine the behavior of the MXY strategy under various scenarios for a stator voltage reference of amplitude $\|\boldsymbol{\nu}\| = 1.85$ p.u. at 46 Hz and 8% slip. Fig. 8(a) shows that, with a healthy VSI, the MXY strategy produces stator currents with $\alpha\beta$ components following a circular trajectory and with negligible xy components. Fig. 8(b) and (c) reveal that, when one cell (a1) or two cells in adjacent phases (a1 and b1) are bypassed, respectively, the MXY strategy preserves the circular trajectory of the $\alpha\beta$ stator currents, while the xy currents are restricted. These experimental measurements align with the simulation results presented in Fig. 4 for $\|\boldsymbol{\nu}\| = 1.85$ p.u.

Fig. 9(a) and (b) presents the harmonic analysis that correspond to the tests depicted in Figs. 7(c) and 8(b), respectively. The top plot in Fig. 9(a) shows that for a reference stator voltage with an amplitude of $\|\boldsymbol{\nu}\| = 1.4$ p.u., the MIN strategy generates a PWM reference with a fundamental amplitude of 1.4 p.u., matching the reference, exhibiting no $\alpha\beta$ harmonics, small zero-sequence harmonics and relatively large xy harmonics. The corresponding bottom plot reveals that these xy harmonics induce substantial xy stator current harmonics due to the low impedance seen by the xy components [14]. The $\alpha\beta$ current harmonics that also arise are attributed to the aforementioned VSI nonlinearities. The top plot in Fig. 9(b) depicts the harmonic components in the PWM reference for a more demanding reference stator voltage, with an amplitude of $\|\boldsymbol{\nu}\| = 1.85$ p.u., which forces the MXY strategy to perform xy injection. Even in this more challenging scenario, the MXY strategy injects lower xy and higher zero-sequence harmonics in the PWM reference compared with the MIN strategy, which results in lower stator current harmonics, as the corresponding bottom plot shows.

Fig. 10 plots the estimated stator copper losses with respect to the rotor speed for the experiments conducted in Figs. 7 and 8, along with the case of using the MXY strategy when the cells a1 and c1 are both bypassed. The speed achievable in these tests is limited by the instantaneous VSI output current. Other hardware

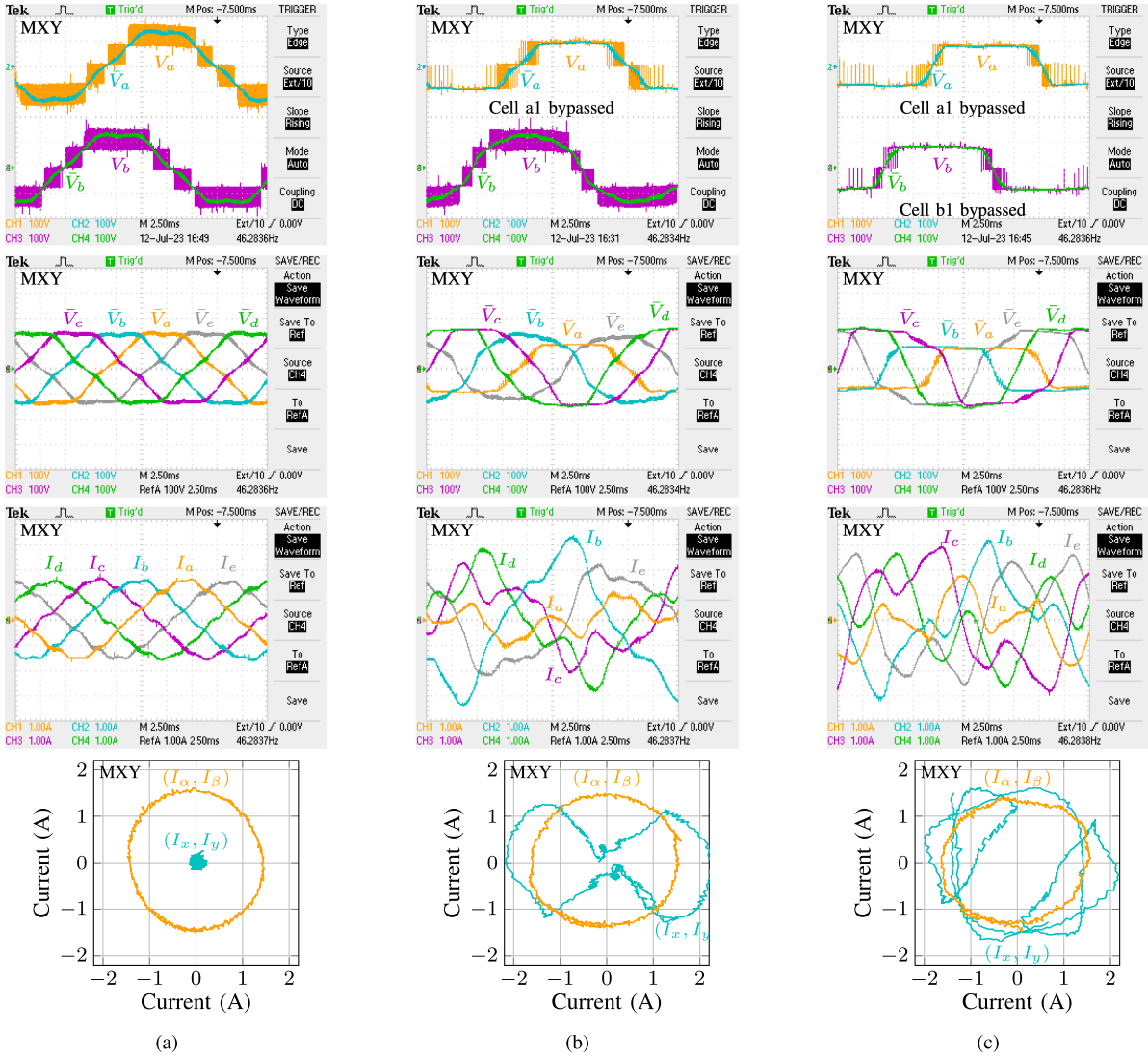

Fig. 8. Experimental measurements for the MXY strategy, $\|\boldsymbol{\nu}\| = 1.85$ p.u., 46 Hz and 8% slip. Raw VSI output voltages, with some waveforms omitted for clarity (top), filtered output voltages (middle top), raw stator currents (middle bottom) and $\alpha\beta$ and xy components of the stator currents (bottom). (a) Healthy VSI. (b) Cell a1 bypassed. (c) Cells a1 and b1 bypassed.

setups could imply different limitations that would require a specific analysis for the maximum achievable speed without field weakening. With the current setup, the MIN strategy with cell a1 bypassed can only be tested up to $976\,\mathrm{r/min}$. This is significantly lower than with the MXY strategy, which reaches $1346\,\mathrm{r/min}$ under the same conditions exhibiting comparable stator copper losses. Notably, the MIN strategy consistently produces significantly higher stator losses than the MXY strategy across all speeds and scenarios tested. In all fault scenarios, the MXY technique does not increase the losses when it does not perform actual xy injection (indicated by dashed lines), compared with the healthy condition. However, when xy components are injected in the PWM reference (indicated by solid lines), the copper losses invariably rise. More importantly, such losses increment aligns with the value of the averaged cost function obtained by simulation, which is presented in Fig. 4. This experimental finding supports the assumption that minimizing the cost function $q(\mathbf{v})$ greatly reduces the stator copper losses.

The machine parameters and the preceding experimental data were used to estimate the electromagnetic torque using the machine model presented in [31]. As shown in Fig. 11(a), for the experiments in Fig. 7 with $\|\boldsymbol{\nu}\| = 1.4$ p.u., both MXY and MIN strategies achieve a similar average torque, of approximately $2.9\,\mathrm{Nm}$. However, the torque ripple increases when using the MIN strategy without an xy filter. This is attributed to the previously mentioned distortion in the $\alpha\beta$ stator current trajectory observed in Fig. 7(c). Similarly, Fig. 11(b) presents the estimated torque for the experiments in Fig. 8. Here, the MXY strategy achieves under different fault scenarios with $\|\boldsymbol{\nu}\| = 1.85$ p.u. an average torque, of roughly $3.4\,\mathrm{Nm}$, and a torque ripple similar to the healthy situation. This aligns with the aforementioned low distortion observed in the circular $\alpha\beta$ stator current trajectories shown in the bottom plots in Fig. 8. In all cases, the effect of the torque ripple on the rotor speed is small, which remains roughly constant during the experiments. Notably, Fig. 11 also demonstrates that, with cells a1 and b1 bypassed, the MXY

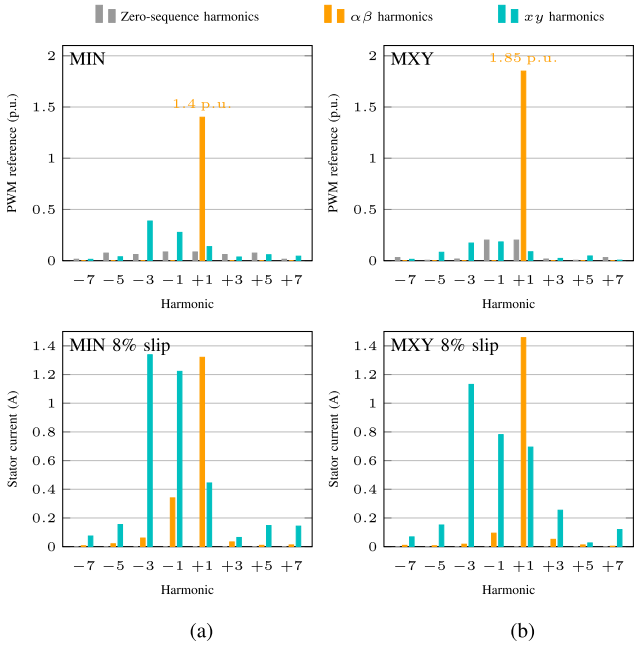

Fig. 9. Harmonic analysis of the PWM voltage reference (top) and the stator currents at 8% slip (bottom). (a) MIN for $\|\boldsymbol{\nu}\| = 1.4$ p.u. at 34 Hz. (b) MXY for $\|\boldsymbol{\nu}\| = 1.85$ p.u. at 46 Hz. The negative sign indicates harmonic components rotating in the opposite direction of the fundamental.

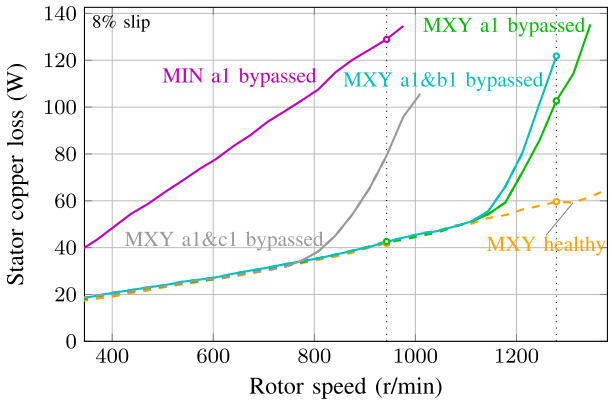

Fig. 10. Experimentally estimated stator copper losses at 8% slip for the MXY and the MIN strategies, normalized with respect to the motor rated values. Dashed lines indicate no actual xy injection in the PWM reference. The highlighted points correspond with the experimental measurements presented in Figs. 7 and 8.

strategy reaches the theoretical limit achievable by the drive in this scenario, without distortion in the $\alpha\beta$ plane or the need for field weakening [3].

The experimental overall drive efficiency, defined as the ratio of estimated mechanical output power to the input dc power and assessed in the cases presented in Fig. 11, aligns with the observed stator copper losses. For the MXY strategy at $\|\boldsymbol{\nu}\| = 1.4$ p.u., the efficiency in healthy conditions is 73.1% and with cell a1 bypassed is 70.5%. Under the same faulty condition, the efficiency with MIN reduces to 49.1%. At $\|\boldsymbol{\nu}\| = 1.85$ p.u. the efficiencies achieved with MXY are 74.2% in

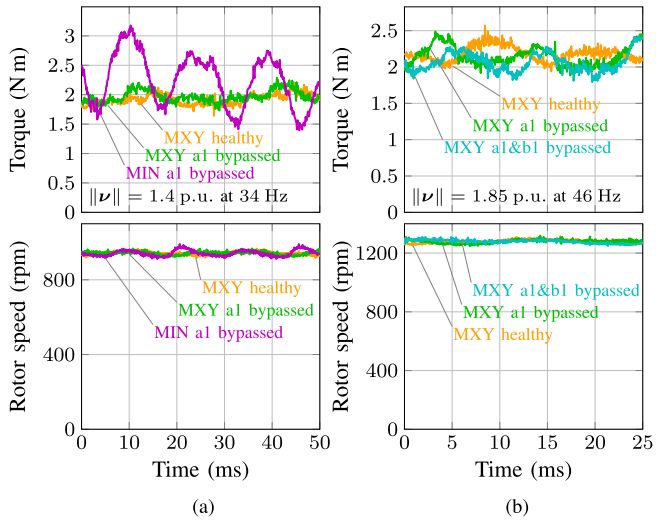

Fig. 11. Experimentally estimated torque and measured rotor speed at 8% slip with (a) MXY and MIN for $\|\boldsymbol{\nu}\| = 1.4$ p.u. at 34 Hz, and (b) MXY for $\|\boldsymbol{\nu}\| = 1.85$ p.u. at 46 Hz.

healthy conditions, 71.1% with cell a1 bypassed and 68.0% with cells a1 and b1 bypassed.

Fig. 12 shows the response of the motor drive with the MXY strategy when cell a1 is bypassed at time $t = 50$ ms for $\|\boldsymbol{\nu}\| = 2.0$ p.u. at 48.8 Hz. Initially, the CHB VSI operates with all cells healthy ($\kappa_a = 2$), thus MXY does not perform any xy injection. In this condition, the measured stator currents exhibit balanced $\alpha\beta$ components with negligible xy components. When the cell a1 is bypassed ($\kappa_a = 1$), MXY prevents $\alpha\beta$ distortion by injecting optimal xy components. The rapid response of the MXY strategy results in negligible disturbance in the electromagnetic torque and rotor speed compared to their natural variations caused by drive nonlinearities.

The box plot in Fig. 13 compares the variation of the execution times with the amplitude of the reference stator voltage $\|\boldsymbol{\nu}\|$ for the MXY task with cold start and the MIN task running on the dSPACE board. This board features a 32-bit PowerPC 604e running at 400 MHz with one floating-point unit, three integer units and 32 kB L1 caches both for instructions and data. The execution time of the MIN task varies slightly between 4.4 μs and 5.8 μs, being nearly independent of $\|\boldsymbol{\nu}\|$. This is explained by the fact that the number of mathematical operations required by the MIN strategy is nearly constant. However, the amount of operations performed by the MXY task depends on the number of iterations required by the proposed active-set algorithm to converge (see Fig. 5). Consequently, Fig. 13 shows that the execution time of MXY exhibits a wider range, varying between 7.1 μs and 15 μs. This is because larger values of $\|\boldsymbol{\nu}\|$ necessitate more iterations to converge, as an increased number of constraints become active at the solution. More importantly, in the worst case, the execution time of the MXY task triples that of the MIN task, disclosing the need for further research to reduce the computational overhead. Nevertheless, this does not necessarily pose a serious limitation for the target applications

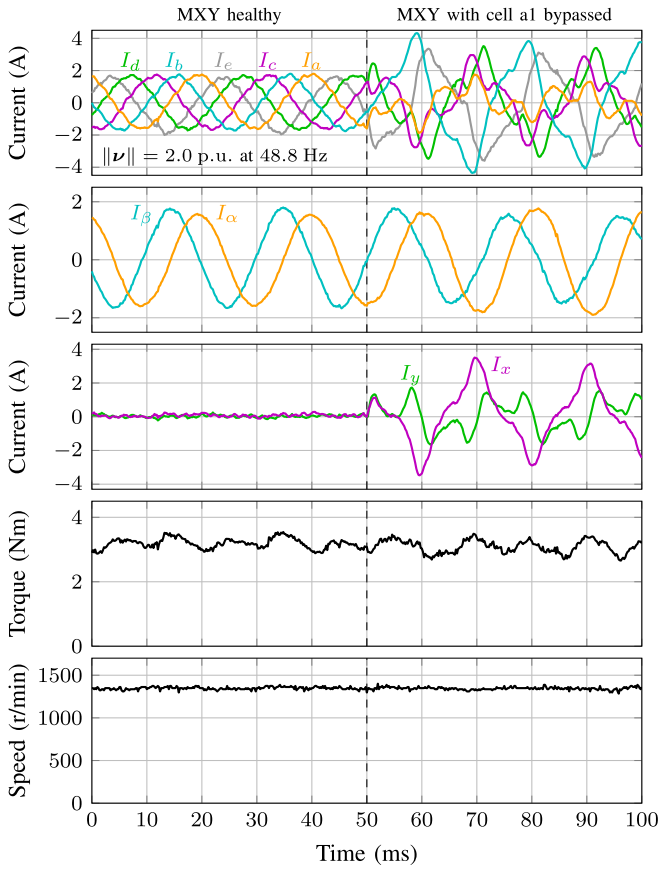

Fig. 12. Transient response with the MXY strategy when one cell is bypassed for $\|\boldsymbol{\nu}\| = 2.0$ p.u. at 48.8 Hz at $t = 50$ ms. Raw stator currents (top), and their $\alpha\beta$ (middle top) and xy (middle) components, estimated electromagnetic torque (middle bottom), and rotor speed (bottom).

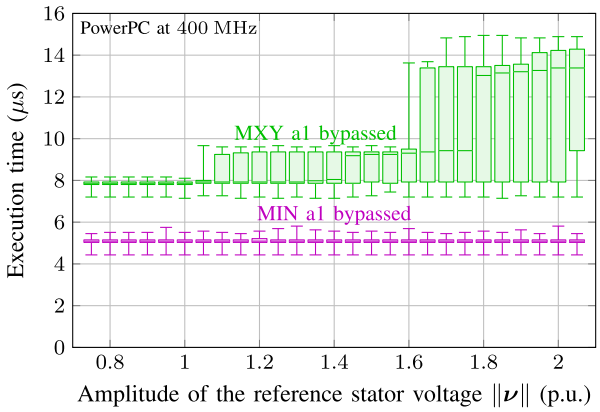

Fig. 13. Execution times of the MXY, with cold start, and the MIN strategies with the cell a1 bypassed. Each box plot indicates the minimum, maximum, median, and first and third quartiles of execution-time data set measured over a fundamental period.

of the proposed technique. Medium-voltage drives based on CHB VSIs [7] utilize powerful control platforms, which can accommodate the higher computational demands of the MXY strategy.

V. Conclusion

This article introduces the MXY postfault strategy, an optimization-based approach to generate optimal PWM reference signals for multiphase motor drives based on CHB VSIs, when certain power cells are bypassed due to faults. The optimal PWM references are determined by exploiting the extra degrees of freedom that exist in multiphase motors, taking into account the constraints introduced by the reduced output voltage range of the phases with bypassed cells. The proposed MXY strategy calculates the optimal PWM reference by injecting the minimum xy components combined with an appropriate zero-sequence needed to maintain the desired $\alpha\beta$ components for the stator voltage. While this approach inevitably introduces low-order xy harmonics into the stator currents, thereby increasing the stator copper losses, the MXY strategy effectively mitigates these unavoidable losses.

The proposed strategy is compared with the MIN alternative, which also employs xy injection but follows a distinct mathematical approach. While MIN was derived by solving an infinity-norm optimization problem and relies on closed-form expressions, MXY is obtained here through an iterative solution of a quadratic problem. Both methods generate the desired $\alpha\beta$ stator voltage without distortion, provided it is compatible with the constraints imposed by bypassed cells of the CHB VSI. However, the MXY strategy exhibits superior performance in terms of stator copper losses and peak currents across all operating conditions and fault scenarios. This significant reduction in losses eliminates the need for the hardware xy filter in the experimental tests, which was recommended for mitigating excessive currents generated by the MIN strategy. While MXY offers substantial advantages, it incurs a higher computational burden. Future research should focus on developing efficient algorithms to mitigate this limitation without compromising the efficacy of the MXY postfault strategy.

Appendix

An efficient method for solving the system of linear equations in (10) at every iteration is necessary to implement the proposed postfault strategy in real time. This linear system can be expressed in matrix form, omitting the iteration index k for the sake of conciseness, as

$$\begin{bmatrix} \mathbf{Q} & \mathbf{A}^{\mathrm{T}} & \mathbf{E}^{\mathrm{T}} \\ \mathbf{A} & \mathbf{0} & \mathbf{0} \\ \mathbf{E} & \mathbf{0} & \mathbf{0} \end{bmatrix} \begin{bmatrix} -\mathbf{p}^* \\ \boldsymbol{\lambda} \\ \boldsymbol{\mu} \end{bmatrix} = \begin{bmatrix} \mathbf{g} \\ \mathbf{h} \\ \mathbf{0} \end{bmatrix} \tag{18a}$$

$$\mathbf{A}^{\mathrm{T}} \stackrel{\mathrm{def}}{=} [\mathbf{c}_\alpha^{\mathrm{T}}, \mathbf{c}_\beta^{\mathrm{T}}] \tag{18b}$$

$$\mathbf{E}^{\mathrm{T}} \stackrel{\mathrm{def}}{=} [\dots, \mathbf{e}_i^{\mathrm{T}}, \dots] \qquad \text{for } i \in \mathcal{L} \cup \mathcal{U} \tag{18c}$$

$$\mathbf{g} \stackrel{\mathrm{def}}{=} \mathbf{Q}\mathbf{v} \tag{18d}$$

$$\boldsymbol{\lambda} \stackrel{\mathrm{def}}{=} [\lambda_\alpha, \lambda_\beta]^{\mathrm{T}} \tag{18e}$$

$$\boldsymbol{\mu} \stackrel{\mathrm{def}}{=} [\dots, \mu_i, \dots, -\mu_j, \dots]^{\mathrm{T}} \qquad \text{for } i \in \mathcal{L} \text{ and } j \in \mathcal{U} \tag{18f}$$

$$\mathbf{h} \stackrel{\text{def}}{=} \mathbf{A}\mathbf{v} - \boldsymbol{\nu} \tag{18g}$$

$$\boldsymbol{\nu} \stackrel{\text{def}}{=} [\nu_\alpha, \nu_\beta]^{\mathrm{T}}. \tag{18h}$$

This system of $n+2+m$ linear equations has to be solved for $\mathbf{p}^*$, $\boldsymbol{\lambda}$ and $\boldsymbol{\mu}$, where m is the size of $\boldsymbol{\mu}$, that is, the number of elements in the set $\mathcal{L} \cup \mathcal{U}$. Recognizing that, according to (10d), some components of $\mathbf{p}^*$ are known to be zero, the vector $\mathbf{p}^*$ can be written as

$$\mathbf{p}^* = \bar{\mathbf{E}}^{\mathrm{T}} \hat{\mathbf{p}}^* \tag{19}$$

where the vector $\hat{\mathbf{p}}^* \stackrel{\text{def}}{=} [\dots, p_i, \dots]^{\mathrm{T}}$, for all $i \notin \mathcal{L} \cup \mathcal{U}$, includes just those unknown components in $\mathbf{p}^*$, and

$$\bar{\mathbf{E}}^{\mathrm{T}} \stackrel{\text{def}}{=} [\dots, \mathbf{e}_i^{\mathrm{T}}, \dots] \quad \text{for } i \notin \mathcal{L} \cup \mathcal{U} \tag{20}$$

is the matrix made with all the standard unit vectors not included in $\mathbf{E}$. If (19) is substituted in (18a), taking into account that $\mathbf{E}\bar{\mathbf{E}}^{\mathrm{T}} = \mathbf{0}$ and $\mathbf{E}\mathbf{E}^{\mathrm{T}} = \mathbf{I}$, being $\mathbf{I}$ the identity matrix, the following system of $n+2$ linear equations is obtained

$$\begin{bmatrix} \mathbf{Q}\bar{\mathbf{E}}^{\mathrm{T}} & \mathbf{A}^{\mathrm{T}} & \mathbf{E}^{\mathrm{T}} \\ \mathbf{A}\bar{\mathbf{E}}^{\mathrm{T}} & \mathbf{0} & \mathbf{0} \end{bmatrix} \begin{bmatrix} -\hat{\mathbf{p}}^* \\ \boldsymbol{\lambda} \\ \boldsymbol{\mu} \end{bmatrix} = \begin{bmatrix} \mathbf{g} \\ \mathbf{h} \end{bmatrix}. \tag{21}$$

The left multiplication of the first block-row equations of this new system by $\mathbf{E}$, leads to the following solution for $\boldsymbol{\mu}$:

$$\boldsymbol{\mu} = \mathbf{E}\mathbf{Q}\bar{\mathbf{E}}^{\mathrm{T}}\hat{\mathbf{p}}^* - \mathbf{E}\mathbf{A}^{\mathrm{T}}\boldsymbol{\lambda} + \mathbf{E}\mathbf{g} \tag{22}$$

which, considering (18d) and (19), can be rewritten as

$$\boldsymbol{\mu} = \mathbf{E}\mathbf{Q}(\mathbf{v} + \mathbf{p}^*) - \mathbf{E}\mathbf{A}^{\mathrm{T}}\boldsymbol{\lambda}. \tag{23}$$

Subsequently, by substituting (22) into (21) and after some manipulations, a reduced system of $n+2-m$ linear equations is obtained

$$\begin{bmatrix} \hat{\mathbf{Q}} & \hat{\mathbf{A}}^{\mathrm{T}} \\ \hat{\mathbf{A}} & \mathbf{0} \end{bmatrix} \begin{bmatrix} -\hat{\mathbf{p}}^* \\ \boldsymbol{\lambda} \end{bmatrix} = \begin{bmatrix} \hat{\mathbf{g}} \\ \mathbf{h} \end{bmatrix} \tag{24}$$

where $\hat{\mathbf{Q}} \stackrel{\text{def}}{=} \bar{\mathbf{E}}\mathbf{Q}\bar{\mathbf{E}}^{\mathrm{T}}$, $\hat{\mathbf{A}} \stackrel{\text{def}}{=} \mathbf{A}\bar{\mathbf{E}}^{\mathrm{T}}$ and $\hat{\mathbf{g}} \stackrel{\text{def}}{=} \bar{\mathbf{E}}\mathbf{g} = \bar{\mathbf{E}}\mathbf{Q}\mathbf{v}$.

This reduced system can be solved by the null-space method [26] by partitioning the vector $\hat{\mathbf{p}}^*$ as

$$\hat{\mathbf{p}}^* = \mathbf{Y}\mathbf{y} + \mathbf{Z}\mathbf{z} \tag{25}$$

where $\mathbf{y}$ and $\mathbf{z}$ are two vector components of $\hat{\mathbf{p}}^*$, and $\mathbf{Y}$ and $\mathbf{Z}$ are two matrices whose columns span the range and the null-space of $\hat{\mathbf{A}}$, respectively. That is, $\hat{\mathbf{A}}\mathbf{Y} = \mathbf{I}$ and $\hat{\mathbf{A}}\mathbf{Z} = \mathbf{0}$ [26]. These two matrices can be calculated as

$$\mathbf{Y} = \mathbf{P}\begin{bmatrix} \mathbf{M}^{-1} \\ \mathbf{0} \end{bmatrix} \tag{26}$$

$$\mathbf{Z} = \mathbf{P}\begin{bmatrix} -\mathbf{M}^{-1}\mathbf{N} \\ \mathbf{I} \end{bmatrix} \tag{27}$$

where $\mathbf{M}$ is a 2×2 submatrix made with any two independent columns of $\hat{\mathbf{A}}$, $\mathbf{N}$ is the submatrix made with all remaining columns of $\hat{\mathbf{A}}$, and $\mathbf{P}$ is defined as the permutation matrix that rearranges the columns of $\hat{\mathbf{A}}$ such that

$$\hat{\mathbf{A}}\,\mathbf{P} \stackrel{\text{def}}{=} [\mathbf{M}|\mathbf{N}]. \tag{28}$$

It is important to remark that all the columns of $\mathbf{A}$, and consequently, all the columns of $\hat{\mathbf{A}}$, are linearly independent for all multiphase motors except for those having an even number of phases with a symmetrical winding arrangement. Therefore, except in these particular cases, a convenient choice for $\mathbf{P}$ is the identity matrix $\mathbf{I}$. If (25) is substituted in (24) taking into account (26) and (27) it results in

$$\mathbf{y} = -\mathbf{h} \tag{29}$$

while $\mathbf{z}$ can be obtained by solving the system of $n-2-m$ linear equations

$$(\mathbf{Z}^{\mathrm{T}}\hat{\mathbf{Q}}\mathbf{Z})\mathbf{z} = \mathbf{Z}^{\mathrm{T}}(\hat{\mathbf{Q}}\mathbf{Y}\mathbf{h} - \hat{\mathbf{g}}) \tag{30}$$

by the Cholesky factorization of the matrix $\mathbf{Z}^{\mathrm{T}}\hat{\mathbf{Q}}\mathbf{Z}$ [26] or directly by using

$$\mathbf{z} = (\mathbf{Z}^{\mathrm{T}}\hat{\mathbf{Q}}\mathbf{Z})^{-1}\mathbf{Z}^{\mathrm{T}}(\hat{\mathbf{Q}}\mathbf{Y}\mathbf{h} - \hat{\mathbf{g}}). \tag{31}$$

Finally, left multiplication of the first block-row in (24) by $\mathbf{Y}^{\mathrm{T}}$, taking into account that $\mathbf{Y}^{\mathrm{T}}\hat{\mathbf{A}}^{\mathrm{T}} = \mathbf{I}$, yields

$$\boldsymbol{\lambda} = \mathbf{Y}^{\mathrm{T}}\hat{\mathbf{Q}}\hat{\mathbf{p}}^* + \mathbf{Y}^{\mathrm{T}}\hat{\mathbf{g}}. \tag{32}$$

Table II summarizes the calculation procedure developed to solve (10) for the optimal step vector $\mathbf{p}^*$ and the Lagrange multipliers $\boldsymbol{\mu}$, which are needed in the algorithm of Section II-D that implements the proposed active-set method for MXY injection.

It is worth noting that matrix multiplications involving $\mathbf{P}$, $\mathbf{E}$ or $\bar{\mathbf{E}}$ can be achieved without performing actual matrix multiplications because they are just row/column rearrangement ($\mathbf{P}$) and row/column selection ($\mathbf{E}$ and $\bar{\mathbf{E}}$) operations. For instance, $\hat{\mathbf{Q}}$ can be obtained by removing the rows and columns of $\mathbf{Q}$ that correspond to indexes not included in the set $\mathcal{L} \cup \mathcal{U}$, while $\hat{\mathbf{A}}$ is equal to $\mathbf{A}$ without the columns that do not match the elements in $\mathcal{L} \cup \mathcal{U}$.

Finally, it is remarked that in some cases the linear system in (18a) may become either overdetermined (possessing no solution) or undetermined (having infinite solutions). The system has no solution when there are not two linearly independent columns in $\hat{\mathbf{A}}$, which thwarts the decomposition presented in (28). This scenario arises when the reference stator vector $\boldsymbol{\nu}$ lays in the overmodulation region, that is, when xy and zero sequence injection cannot prevent distortion in the $\alpha\beta$ plane. Conversely, the system has infinite solutions when the matrix $\mathbf{Z}^{\mathrm{T}}\hat{\mathbf{Q}}\mathbf{Z}$ is singular. In this case, there exist infinite optimal solutions, all of which yield the same value of the cost function $q(\mathbf{v})$ but differ solely in the zero-sequence component. One such optimal solution can be obtained by calculating a PWM reference vector $\mathbf{v}$, either by no xy injection at all or by clamping at least one phase in every group of isolated windings, followed by the injection of an appropriate zero-sequence (e.g., the generalized min–max injection by Carnielutti [3], [28]).

REFERENCES

[1] J. Rodr, P. W. Hammond, J. Pontt, R. Musalem, P. Lezana, and M. J. Escobar, "Operation of a medium-voltage drive under faulty conditions," *IEEE Trans. Ind. Electron.*, vol. 52, no. 4, pp. 1080–1085, Aug. 2005.

[2] A. G. Yepes, Ó. López, I. González-Prieto, M. J. Durán, and J. Doval-Gandoy, "A comprehensive survey on fault tolerance in multiphase AC drives. Part 1: General overview considering multiple fault types," *Machines*, vol. 10, no. 3, Mar. 2022, Art. no. 208.

[3] Ó. López, et al., "Post-fault operation strategy for cascaded H-bridge inverters driving a multiphase motor," *IEEE Trans. Ind. Electron.*, vol. 71, no. 5, pp. 4309–4319, May 2024.

[4] H. Abu-Rub, S. Bayhan, S. Moinoddin, M. Malinowski, and J. Guzinski, "Medium-voltage drives: Challenges and existing technology," *IEEE Power Electron. Mag.*, vol. 3, no. 2, pp. 29–41, Jun. 2016.

[5] M. Malinowski, K. Gopakumar, J. Rodr, and M. A. Pérez, "A survey on cascaded multilevel inverters," *IEEE Trans. Ind. Electron.*, vol. 57, no. 7, pp. 2197–2206, Jul. 2010.

[6] M. Vijeh, M. Rezanejad, E. Samadaei, and K. Bertilsson, "A general review of multilevel inverters based on main submodules: Structural point of view," *IEEE Trans. Power Electron.*, vol. 34, no. 10, pp. 9479–9502, Oct. 2019.

[7] "Medium voltage drives, SINAMICS perfect harmony GH180," Siemens, Tech. Rep., Feb. 2022.

[8] P. Lezana, J. Pou, T. A. Meynard, J. Rodríguez, S. Ceballos, and F. Richardeau, "Survey on fault operation on multilevel inverters," *IEEE Trans. Ind. Electron.*, vol. 57, no. 7, pp. 2207–2218, Jul. 2010.

[9] P. W. Hammond, "Enhancing the reliability of modular medium-voltage drives," *IEEE Trans. Ind. Electron.*, vol. 49, no. 5, pp. 948–954, Oct. 2002.

[10] P. Lezana and G. Ortiz, "Extended operation of cascade multicell converters under fault condition," *IEEE Trans. Ind. Electron.*, vol. 56, no. 7, pp. 2697–2703, Jul. 2009.

[11] F. Carnielutti and H. Pinheiro, "Hybrid modulation strategy for asymmetrical cascaded multilevel converters under normal and fault conditions," *IEEE Trans. Ind. Electron.*, vol. 63, no. 1, pp. 92–101, Jan. 2016.

[12] A. Mora, P. Lezana, and J. Juliet, "Control scheme for an induction motor fed by a cascade multicell converter under internal fault," *IEEE Trans. Ind. Electron.*, vol. 61, no. 11, pp. 5948–5955, Nov. 2014.

[13] S. Ouni, M. Narimani, Z. Cheng, and N. R. Zargari, "A new postfault control method for CHB inverter to increase maximum output voltage," *IEEE Trans. Ind. Appl.*, vol. 56, no. 5, pp. 5499–5510, Sep./Oct. 2020.

[14] E. Levi, "Advances in converter control and innovative exploitation of additional degrees of freedom for multiphase machines," *IEEE Trans. Ind. Electron.*, vol. 63, no. 1, pp. 433–448, Jan. 2016.

[15] E. A. Klingshirn, "High phase order induction motors — Part I-description and theoretical considerations," *IEEE Trans. Power Appl. Syst.*, vol. PAS-102, no. 1, pp. 47–53, Jan. 1983.

[16] A. Shawier, A. S. Abdel-Khalik, R. A. Hamdy, K. H. Ahmed, and S. Ahmed, "Postfault operation of five-phase induction machine with minimum total losses under single open-phase fault," *IEEE Access*, vol. 8, pp. 208696–208706, 2020.

[17] M. J. Durán, J. Prieto, and F. Barrero, "Space vector PWM with reduced common-mode voltage for five-phase induction motor drives operating in overmodulation zone," *IEEE Trans. Power Electron.*, vol. 28, no. 8, pp. 4030–4040, Aug. 2013.

[18] G. Carrasco and C. A. Silva, "Space vector PWM method for five-phase two-level VSI with minimum harmonic injection in the overmodulation region," *IEEE Trans. Ind. Electron.*, vol. 60, no. 5, pp. 2042–2053, May 2013.

[19] H. Liu, D. Wang, X. Yi, X. Zheng, X. Yu, and B. Pan, "Loss reduction of five-phase induction motor with third harmonic injection throughout widest torque range under open-circuit faults," *IEEE Trans. Emerg. Sel. Topics Power Electron.*, vol. 11, no. 5, pp. 4643–4658, Oct. 2023.

[20] A. G. Yepes, A. Shawier, W. E. Abdel-Azim, A. Abdel-Khalik, S. Ahmed, and J. Doval-Gandoy, "General online current-harmonic generation for increased torque capability with minimum stator copper loss in fault-tolerant multiphase induction motor drives," *IEEE Trans. Transp. Electrific.*, vol. 9, no. 3, pp. 4650–4667, Sep. 2023.

[21] M. Medina-Sánchez, A. G. Yepes, Ó. López, and J. Doval-Gandoy, "Assessment and exploitation of the minimum current harmonic distortion under overmodulation in five-phase induction motor drives," *IEEE Trans. Power Electron.*, vol. 38, no. 4, pp. 4289–4305, Apr. 2023.

[22] M. Medina-Sánchez, A. G. Yepes, Ó. López, A. S. Abdel-Khalik, and J. Doval-Gandoy, "A carrier-based overmodulation strategy with minimum voltage distortion for symmetrical n-phase induction motor drives," *IEEE Trans. Power Electron.*, vol. 38, no. 12, pp. 15055–15071, Dec. 2023.

[23] L. Vancini, M. Mengoni, G. Rizzoli, G. Sala, L. Zarri, and A. Tani, "Carrier-based PWM overmodulation strategies for five-phase inverters," *IEEE Trans. Power Electron.*, vol. 36, no. 6, pp. 6988–6999, Jun. 2021.

[24] D. C. White and H. H. Woodson, *Electromechanical Energy Conversion*. Cambridge, MA, USA: MIT Press, Nov. 1968.

[25] E. Levi, "Multiphase electric machines for variable-speed applications," *IEEE Trans. Ind. Electron.*, vol. 55, no. 5, pp. 1893–1909, May 2008.

[26] J. Nocedal and S. Wright, *Numerical Optimization*. Berlin, Germany: Springer-Verlag, 2006.

[27] N. I. M. Gould and P. L. Toint, "Numerical methods for large-scale non-convex quadratic programming," in *Proc. 1st Int. Conf. Ind. Appl. Math. Indian Subcontinent*, 2002, pp. 149–179.

[28] F. Carnielutti, H. Pinheiro, and C. Rech, "Generalized carrier-based modulation strategy for cascaded multilevel converters operating under fault conditions," *IEEE Trans. Ind. Electron.*, vol. 59, no. 2, pp. 679–689, Feb. 2012.

[29] D. G. Holmes and T. A. Lipo, *Pulse Width Modulation for Power Converters: Principles and Practice*. Hoboken, NJ, USA: Wiley, 2003.

[30] A. Mora, J. Juliet, A. Santander, and P. Lezana, "Dead-time and semiconductor voltage drop compensation for cascaded H-bridge converters," *IEEE Trans. Ind. Electron.*, vol. 63, no. 12, pp. 7833–7842, Dec. 2016.

[31] L. Vancini, M. Mengoni, G. Rizzoli, L. Zarri, and A. Tani, "High-torque density and voltage overmodulation for five-phase induction motor drives," *IEEE Trans. Ind. Appl.*, vol. 4, no. 4, pp. 6291–6298, Jul./Aug. 2024.

Óscar López (Senior Member, IEEE) received the M.Sc. and the Ph.D. degree in electrical engineering from Universidade de Vigo, Vigo, Spain, in 2001 and 2009, respectively.

Since 2004, he has been an Associate Professor with the Universidade de Vigo. His research interest are in the areas of ac power conversion.

Dr. López is a member of the Applied Power Electronics Technology Research Group, Universidade de Vigo.

Jacobo Álvarez was born in Vigo, Spain, in 1967. He received the Ph.D. degree in electronics from Universidade de Vigo, Vigo, Spain, in 1995.

He is currently an Engineer with the University of Vigo, Vigo, in 1991. He has been an Associate Professor with the University of Vigo since 1997. His main topics of interest are Programmable Logic Devices and Field Programmable Gate Arrays architectures and design methods, applied to industrial control problems.

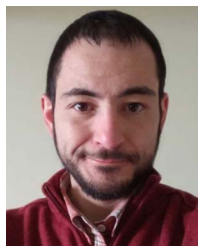

Alejandro G. Yepes (Senior Member, IEEE) received the M.Sc. and Ph.D. degrees in electrical engineering from Universidade de Vigo, Vigo, Spain, in 2009 and 2011, respectively.

Since 2008, he has been with the Applied Power Electronics Technology Research Group, Universidade de Vigo. From 2016 to 2018, he was a visiting scholar with the Department of Electrical and Computer Engineering, Texas A&M University, College Station, TX, USA. His research interests are in the areas of ac power conversion, with special focus, currently, on multiphase machine drives.

Martín Medina-Sánchez received the M.Sc. degree in electrical engineering from the Escuela Superior Politécnica de Chimborazo, Riobamba, Ecuador, in 2017. He is currently working toward the Ph.D. degree in electrical engineering with the Applied Power Electronics Technology Research Group (APET), Universidade de Vigo.

His research interests include multiphase drives and power electronics.

Jesús Doval-Gandoy (Member, IEEE) received the M.Sc. degree from the Polytechnic University of Madrid, Madrid, Spain, in 1991, and the Ph.D. degree from Universidade de Vigo, Vigo, Spain, in 1999, both in electrical engineering.

He is currently a Professor and the Head of the Applied Power Electronics Technology Research Group (APET), Universidade de Vigo. His research interest includes ac power conversion.